

# Comparative Study of the Tribological Behavior of Brass Alloys Produced by Different Manufacturing Processes

N. Bouzayeni · M. Kchaou · R. Elleuch ·  
V. S. Aigbodion

Submitted: 26 September 2012/in revised form: 22 May 2013/Published online: 10 July 2013  
© ASM International 2013

**Abstract** This paper presents an experimental investigation of the tribological behavior of four brass alloys' synthesis by forging (Mm), free-cutting (Md), gravitational casting (Mc), and casting under pressure (Mi). The experiments were conducted on a pin-on-disk tribometer with a load of 200 N, sliding speed of 2.5 m/s, and a sliding distance of 500 m. The microstructure and the worn surfaces were examined with an optical and scanning electron microscope. The results obtained show that the Mc material has less wear resistance related to the presence of voids and an abrasive wear mechanism and the Md material has a stabilized friction coefficient which is related to the uniform distribution of the various phases in the microstructure and the presence of a thick layer of metal transfer on the counter material.

**Keywords** Brass alloys · Severe friction conditions · Tribological performance · Manufacturing process

## Introduction

Brass and its alloys are the materials which are widely used in friction parts of machines, such as bearing liners and

synchronizer rings [1, 2]. Properties such as high strength and hardness, fatigue strength, wear resistance, etc., are required for these materials, and it is important to investigate their tribological behavior [3, 4].

Research has been conducted on the effects of microstructure and environmental conditions on the wear brass alloy [5, 6]. Elleuch et al. [7] studied the different forming processes of brass such as forging, free-cutting, gravitational casting, and casting under pressure; considerable changes are observed in tribological characteristics of the sliding contact. The choice of approved material for an industrial application should be optimized with its friction and wear properties to insure high service performance [8]. The friction characterization depends on the measurement system and the chosen test device. Most of the authors use a pin-on-disk tribometer to characterize their materials [9, 10]. Analyses of the surface layer formed on dry sliding against steel AISI 1045 have shown good correlation such as hardness and wear resistance [8]. It is assumed that wear processes are mainly determined by mechanisms of surface film formation and destruction. For brass and steel, plastic deformation plays an important role in the wear mechanism in different atmospheres [11, 12].

In this work, an attempt has been made to study the tribological behavior of four brass alloys produced from four different method (forging, free-cutting, gravitational casting, and casting under pressure). Their wear behaviors were examined using a pin-on-disk tribometer, developed specially for this purpose. The effects of sliding speed and normal load on the friction and wear performance were investigated. Moreover, the composition and microstructure of worn surfaces of the specimens were analyzed by optical images and a scanning electron microscope (SEM).

---

N. Bouzayeni · M. Kchaou · R. Elleuch (✉)  
ENIS, LASEM, University of Sfax, Route de Soukra km 4,  
3038 Sfax, Tunisia  
e-mail: riadh.elleuch@gnet.tn

V. S. Aigbodion  
Department of Metallurgical and Materials Engineering,  
University of Nigeria, Nsukka, Nigeria

## Architecture and Specificity of the Developed Tribometer

Figure 1 shows a picture of the developed tribometer. The purpose of this tribometer is to measure the friction properties of dry friction contact for different loading and sliding speed conditions. The developed tribometer must therefore satisfy the following functional requirements: it must be able to (i) apply a constant speed, (ii) apply and measure different normal forces, and (iii) measure accurately the friction force acting between the counter materials.

The instrument of the tribometer can be divided into four parts: an actuator part (containing components 1 and 7), a friction part (components 6, 11, and 12), a loading part (components 4 and 5), and a temperature part (components 8, 9, 13, and 14). The different parts are decoupled as much as possible: The actuation part and frictional part are only coupled by the frictional interface under investigation. The structure of the machine and the parallel plates was constructed precisely to insure the levelness of the contact faces and the important rigidity of the structure. The disk is driven by an electric motor which provides rotational movement of a sample holder. A centering mechanism was designed in the sample holder to keep the sample centered with respect to the axis of the machine. The data acquisition system (component 9) is accurate enough to collect several data points in a fraction of a second in order to sense the frictional force before and after sliding in order to differentiate between the static and dynamic coefficients of friction. Friction curves can be constructed in a short-term test with a few rotations of the sample. The tribometer can also be applied for long-term tests in which wear occurs and the friction curve extends throughout the test. In this case, the traveled distance can be kilometers and the

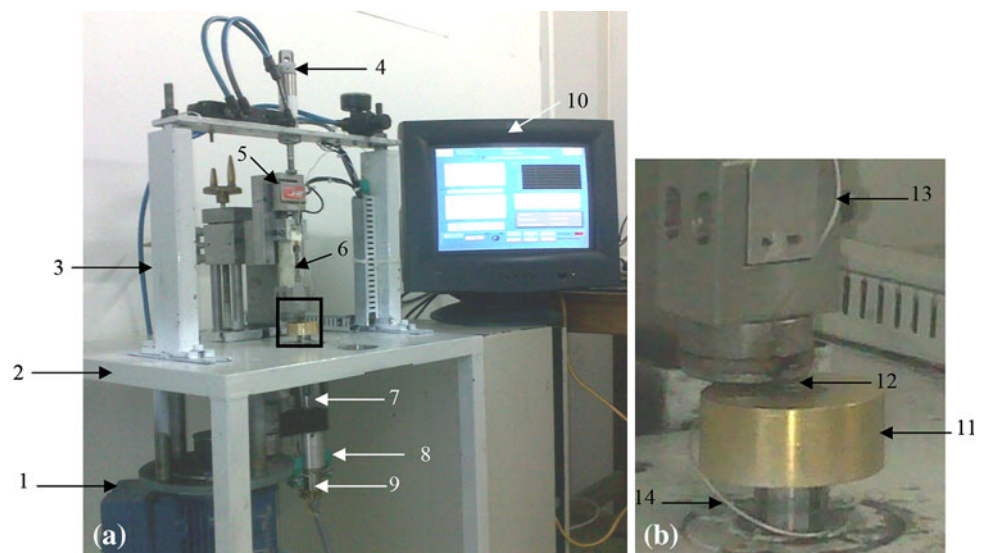
elapsed time can be in the range of hours. At the end of a wear test, the weight loss is a measure of wear rate can be measured by an accurate scale.

The specimen (pin and disk) geometry is shown in Fig. 1b. The mounting place of the thermocouple in the pin (compound 13) is also shown in the same figure. The disk corresponds to the brass alloy and the pin is an antagonist material. The normal load  $P$  and the frictional force  $F$  are measured, respectively, using a load cell having a capacity of 500 N and a strain gage; then, the mean sliding friction coefficient  $\mu$  can be obtained. The calibrated system calculated the friction coefficient by dividing the frictional force by normal load. During the experiment, the temperatures of the contact surfaces of the pin and the disk are measured. The environmental temperature  $T$  is 21–25°C. The plated thermocouples are inserted 2 mm under the specimen surface (Fig. 1). The mean temperature of the frictional surface is evaluated through the value of surface temperature measured according to an approximate formula.

## Materials and Specimen Preparation

Brass alloys of composition 58 wt% Cu, 39 wt% Zn, and 3 wt% Pb were produced from four different processes: forging, free-cutting, gravitational casting, and casting under pressure, noted as Mm, Md, Mc, and Mi, respectively. The samples for metallographic examination were prepared prior to each test; the samples were ground with 1500 grit SiC emery paper and cleaned in acetone using an ultrasonic bath for 10 min and dried in hot air. The microstructural features were examined before and after wear testing using optical microscopy. After each wear test, the metallographic samples were obtained by

**Fig. 1** (a) Picture of the developed tribometer, (b) Specimens (pin and disk) (1. Motor, 2. Table, 3. Guidance, 4. Pneumatic loading, 5. Normal force sensor, 6. Transducer, 7. Spindle, 8. Four thermocouples type K, 9. Slip ring, 10. Acquisition, 11. Disk, 12. Pin, 13, and 14. Thermocouples type K)



sectioning the disk perpendicular to the surface contact. Morphologies of the worn surfaces after wear tests were also examined using a SEM in the secondary electron mode.

A multi-specimen was used for the wear test rig on the pin-on-disk tribometer. The pin specimen had a spherical shape with a diameter of 10 mm. The pin was kept stationary, while the circular disk was rotating. The disk had a 50 mm diameter and 25 mm thickness. In order to get the same condition of the sliding surface in successive tests, the pin and the disk were replaced before each experiment. The sliding speed was fixed at 2.5 m/s, the constant normal load was 200 N, and the sliding distance was chosen up to 500 m. The wear resistance was measured by the weight loss technique using a microbalance with an accuracy of  $\pm 0.02$  mg.

## Results and Discussion

The optical microstructure of the four brass alloys is shown in Fig. 2. The microstructure analysis of the brass CuZn39Pb3 shows a global duplex alpha–beta structure, containing a dispersion of fine lead particles, which is distributed inter-dendritically in the copper alloy as small globules (see Fig. 2), but some differ from one process to the other:

- The structure of the brass from forging is characterized by elongated grains with slip bands (see Fig. 2a) in a specific direction. The largest grains are that of the alpha phase of the average size near 150  $\mu\text{m}$  and that of the beta phase slightly below 30  $\mu\text{m}$ .
- Free-cutting process induces a complex microstructure with brittle phases' precipitate from the matrix, probably during extensive heating or from transformation mechanisms leading to new microconstituents (see Fig. 2b). It contained remarkably fine and uniform  $\alpha$ ,  $\beta$  phases with an average grain size of 20  $\mu\text{m}$  and precipitates at the grain boundaries having a mean particle size of 0.5  $\mu\text{m}$  diameter, which were dispersed in both phases.
- Gravitational casting structure shows dendrites of alpha (dark) in a matrix of beta (white) (see Fig. 2c).
- Figure 2d shows the microstructures of the brass casting under presser with dendritic grains. The bigger grain size creates a coarse microstructure, having less alloy segregation.

For the two last processes, as the grain size decreases, the strength and the ductility of the cast alloy increase, microporosity in the casting decreases, and the tendency for the casting to crack during the solidification decreases. However, the lack of uniformity in grain size and

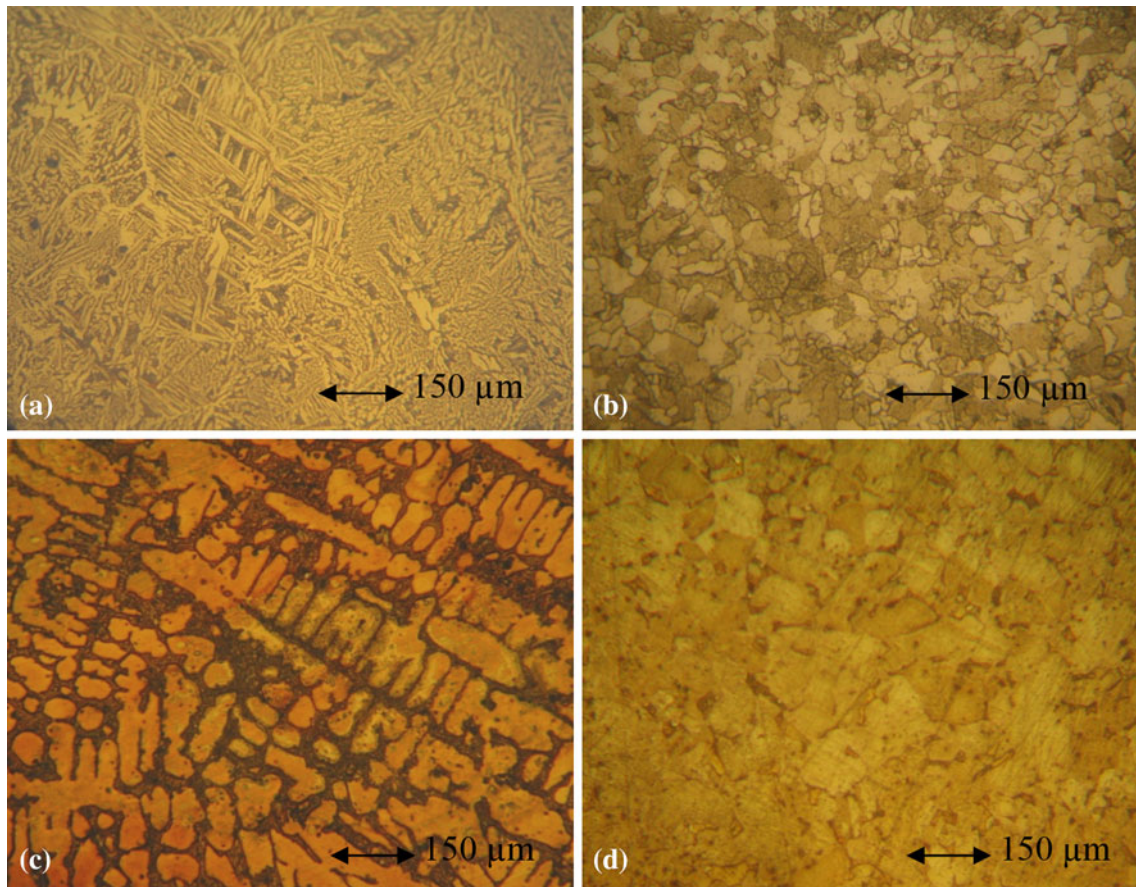
distribution results in castings with anisotropic properties. Grain size has a significant effect on the strength of metals. The smaller the grain size, the stronger the metal [13]. The chemical composition, initial surface roughness, and hardness values of the brass alloys are given in the Table 1. Table 2 shows the mechanical properties of the brass alloys. It was observed that the Md material is more hard and relatively stronger than the other alloys; this may be attributed to the more uniform structure of Md (see Fig. 2b).

Figure 3 shows the friction coefficient ( $\mu$ ) as a function of the sliding distance— $\mu_i$ : casting under pressure;  $\mu_c$ : gravitational casting;  $\mu_m$ : forging;  $\mu_d$ : free-cutting. The friction coefficient curves show a three-phase evolution for each material: The first friction coefficient varied between 0.2 and 0.27. Then,  $\mu$  increases up to 0.35. A small difference is detected in the first step and a large difference is observed specially at the end of the second and the third steps. The variation of  $\mu$  is essentially controlled by the mechanical properties of the brass film that was formed; a rapid decrease in shear strength leads to a decrease in friction load. The friction coefficient is relatively high (0.27) at the beginning of the sliding for the Mm material, but it decreases rapidly in a sliding distance of 20 m, so that it reaches a limiting value of 0.2 in the beginning of the second step and 0.4 as an average in the final step. The Md material shows the most stabilized  $\mu$ , about 0.25 for all the steps. From this analysis, we can affirm that, on middle pressure, the friction coefficient for brass/steel couple presents two transition zones, on 35 and 400 m of the sliding distance in spite of the structure difference.

The quantification of the weight loss of the samples Mc, Mi is Mm are similar; about 1.96 g, whereas for Md, it is 2.2 g. Thereafter, the free-cutting processed alloy showed better wear resistance. It can be concluded from this result that the weight loss in the middle sliding condition increased with the size of the grain induced by the forming process. This can be explained mainly by the improved hardness and impact toughness of the alloy as well as the morphological changes in the brass phase [14].

Figures 4 and 5 show the temperature evolution on the pin and the disk in relation with the sliding distance. For the pin, the temperature increases continually from 30 to 90°C for the four alloys, while the disk temperature evolution. It was observed that the Mm brass alloy was heated more than the other materials; the temperature of the Mm alloy increases up to 210°C at the end of the test, while the other brass alloy study has a limited increase up to 170°C. Instantaneous surface temperature variation (Figs. 4, 5) against sliding distance shows a continuous jump for both friction coefficient and temperature. However, the fluctuation of the friction coefficient in the step III (Fig. 3) with increasing sliding distance can be attributed to the





**Fig. 2** Variation of microstructure with elaboration process: (a) forging (Mm), (b) free-cutting (Md), (c) gravitational casting (Mc), (d) casting under pressure (Mi)

**Table 1** Chemical composition and surface characteristic of different brass alloys

Material	Chemical composition	Initial surface roughness, μm	Hardness HV
Md	58 wt% Cu, 39 wt%, Zn 3 wt% Pb	0.2–0.3	155 (5)
Mc	58 wt% Cu, 39 wt%, Zn 3 wt% Pb	0.2–0.3	102 (3)
Mi	58 wt% Cu, 39 wt%, Zn 3 wt% Pb	0.2–0.3	120 (5)
Mm	58 wt% Cu, 39 wt%, Zn 3 wt% Pb	0.2–0.3	110 (5)

The numbers in parentheses correspond to measurement variation

formation of oxide film on the worn surface [15]. The temperature rise due to friction heat increased the oxidation rate and led to the formation of an oxide film spreading on the surface, which might adhere well to the surface below and thus acted as a solid lubricant, resulting in the reduction of friction coefficient.

The global mass loss measured at the end of the test is shown in Fig. 6. It can be seen that the Mc material had

**Table 2** Mechanical properties of different brass alloys from tensile test

Material	Rm, MPa	Rp0.2, MPa	A, %
Md	510 (10)	440 (10)	8 (5)
Mc	440 (10)	314 (10)	25 (5)
Mi	390 (10)	265 (10)	30 (5)
Mm	370 (10)	160 (10)	35 (5)

The numbers in parentheses correspond to measurement variation

less wear resistance, whereas the Md had excellent resistance to wear showed by less weight loss. This behavior will be explicated by the wear mechanism in the next section.

The morphology of the worn surfaces is shown in Fig. 7. The wear surface of the gravitational casting alloy sample Mc is fully covered by parallel sliding tracks and fine particles (Fig. 7b), whereas the forging alloy sample Mm revealed mainly scratches and deep grooves with the presence of large and lengthy third bodies (Fig. 7c). The morphology of the worn surface of the free-cutting Md sample was somewhat different and the surface showed

**Fig. 3** Friction coefficient evolution in step with sliding distance (normal loading: 200 N; Speed: 1000 rpm).  $\mu_c$ , gravitational casting;  $\mu_i$ , casting under pressure;  $\mu_d$ , free-cutting;  $\mu_m$ , forging

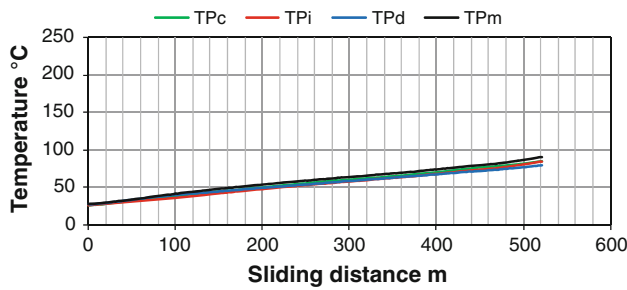
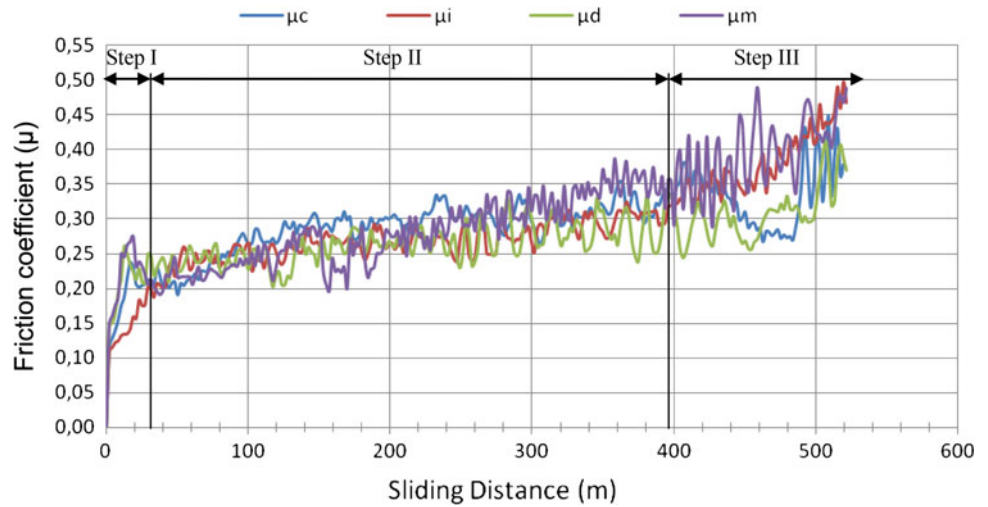


**Fig. 4** Temperature evolution of pins in step with sliding distance. TDC, gravitational casting; TDI, casting under pressure; TDD, free-cutting; TDM, forging

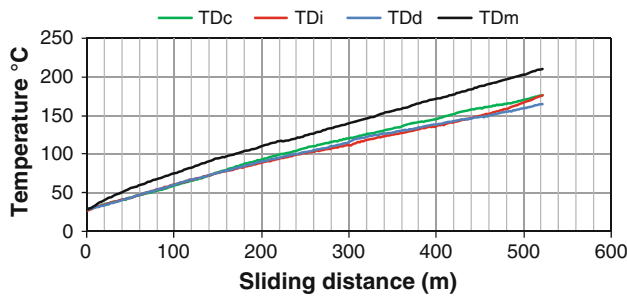


**Fig. 5** Temperature evolution of disk in step with sliding distance. TDC, gravitational casting; TDI, casting under pressure; TDD, free-cutting; TDM, forging

mainly smearing and adhering of worn debris with limited wear tracks (Fig. 7d). This shows that the structure of these materials changed the main wear mechanism of the alloys, and adhesive-type wear mechanism is dominant. This is because the worn materials in the processed samples are mostly smeared on the rubbing surface instead of leaving from the sliding surfaces due to the transfer metal to the pin. Scratches and deep grooves observed on the surfaces are caused by the abrasive action of hard debris particles, such as fragmented particles, brass, and oxidized metal that

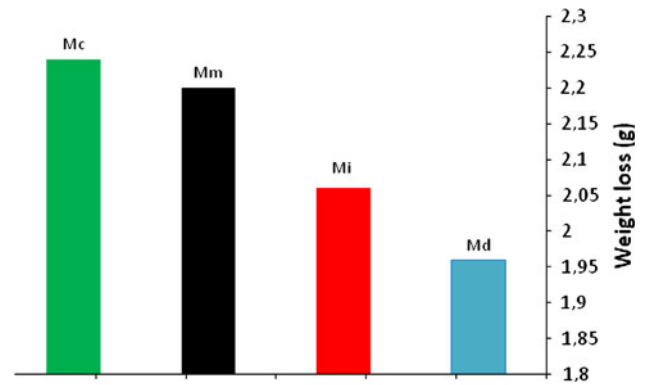


**Fig. 6** Materials' weight loss

was removed from the specimen surface, and by machining chips of iron detached from the steel pin in due course of sliding. Such particles get entrapped in between the mating surfaces causing abrasion. The main wear mechanism observed in the Mc and Mm alloy is abrasion. The wear mechanism of the brass alloys was analyzed by SEM observations (see Fig. 8).

Figure 8a shows two areas on the surface: slip bands and streaks of wear to alternate in the direction of slip. Bands appear smooth and have straight traces that show the contact. The depth of the grooves does not exceed a few microns; debris was also observed. Their sizes are variable up to 50  $\mu\text{m}$  (Fig. 8b). In Fig. 8c, large fragmented particles are observed; the detachment of the transfer layer brings up a rough surface. This behavior reflects a transfer mechanism that occurred between the disk and the pin in the contact.

Figure 9 shows SEM observations of a rubbed surface of Mc brass alloy. As illustrated in Fig. 8a, b, there are slip bands and small clusters of locally fragmented particles. Wear striations also appear in this region. In another area, voids are detected, revealing a porous surface with different

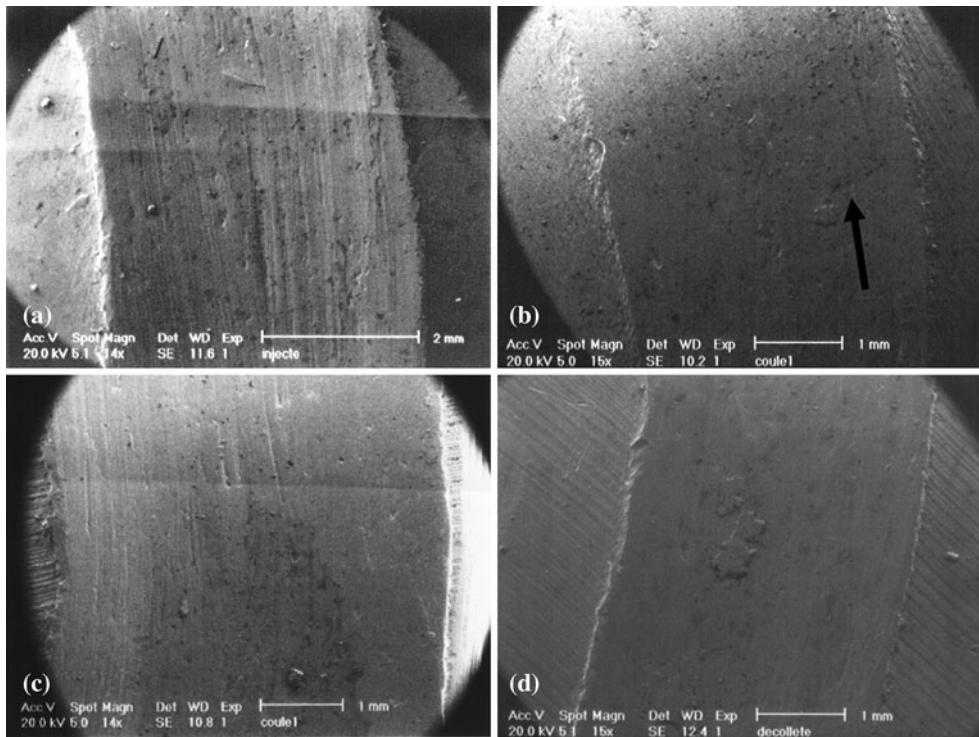


Fig. 7 SEM observations of worn surface; (a) Mi, (b) Mc, (c) Mm, (d) Md brass

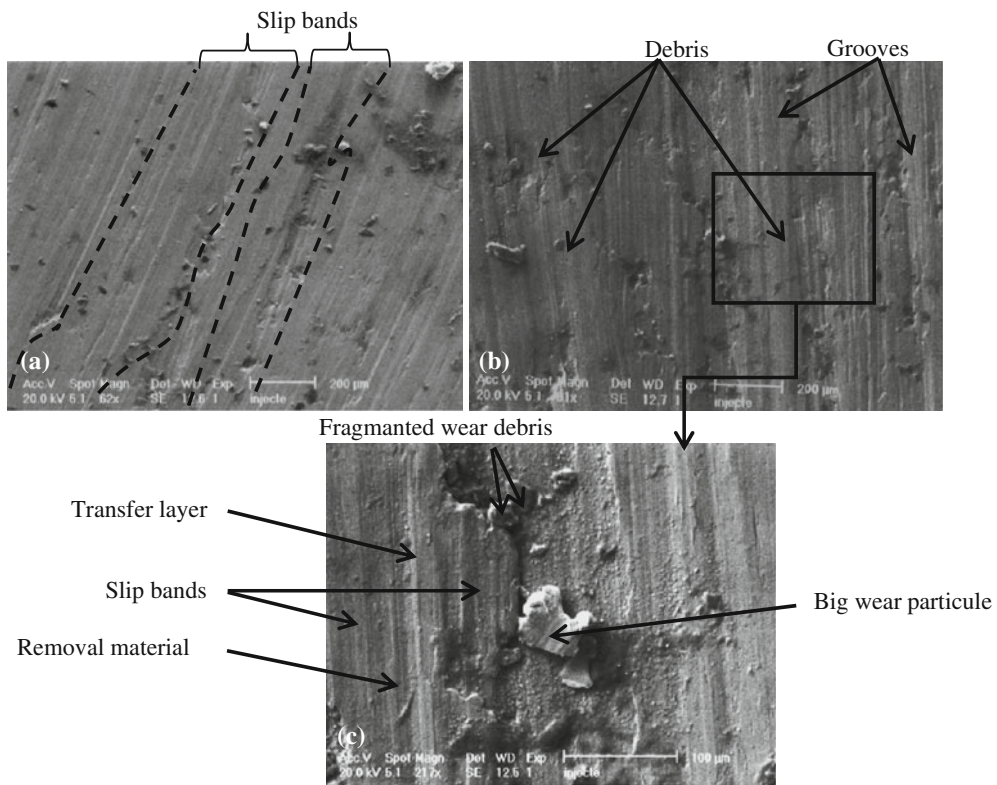
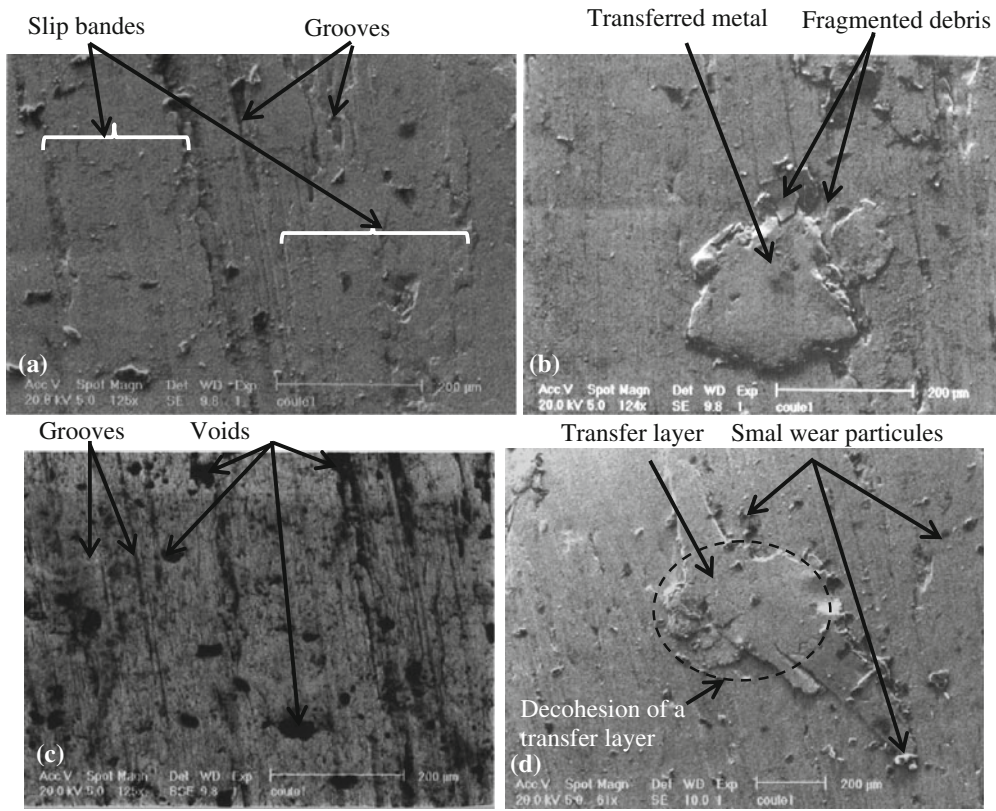
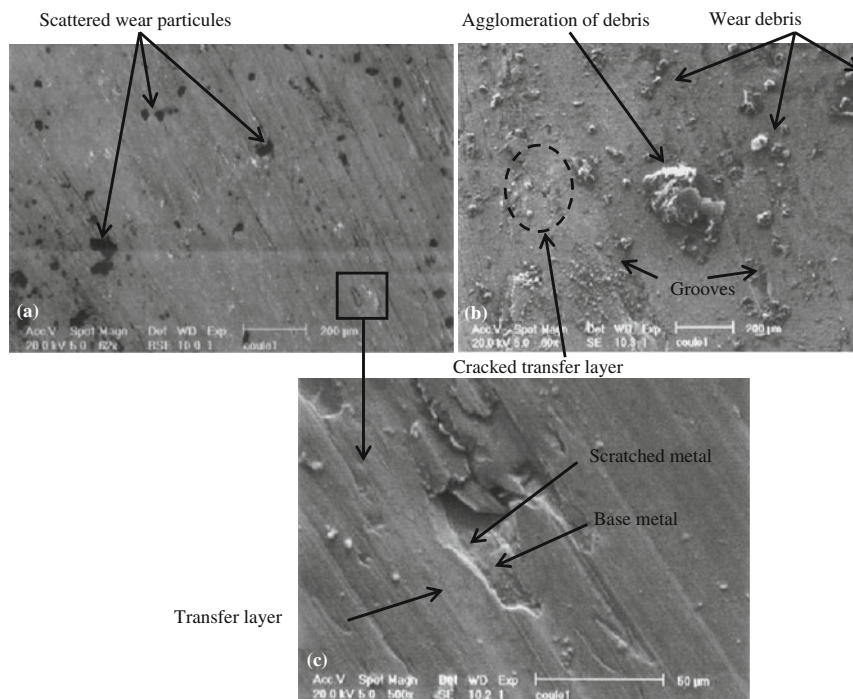


Fig. 8 SEM observations of Mi brass: (a) and (b) two different zones of the rubbed surface showing band structure, (c) detail of wear grooves





**Fig. 9** SEM observations of sliding trace of Mc brass: (a) band structure of the rubbed surface, (b) localization of big debris, (c) surface full of voids, (d) decohesion of a transfer layer



**Fig. 10** SEM observations of sliding trace of Mc brass: (a) smooth surface, (b) rough surface, (c) scratched surface

diameters and large stretching up to 20 μm. Near this area, a metal transfer is detected spread in the sliding direction and fine particles are attached to the surface, while others are cracked, with detachment of the transfer layer (Fig. 9c). From these analyses, the following can be observed:

- A metal transfer mechanism dominates the wear behavior of Mc brass.

- The presence of pores and voids close to the pile of debris accelerates the mechanism of metal tearing, facilitated by the porous structure. This manufacturing defect accelerates the wear of brass, which when detached is driven by friction and compacted to form a transfer layer. Once it reaches a critical size of cracks, it thereby promotes the launch of the transfer layer of

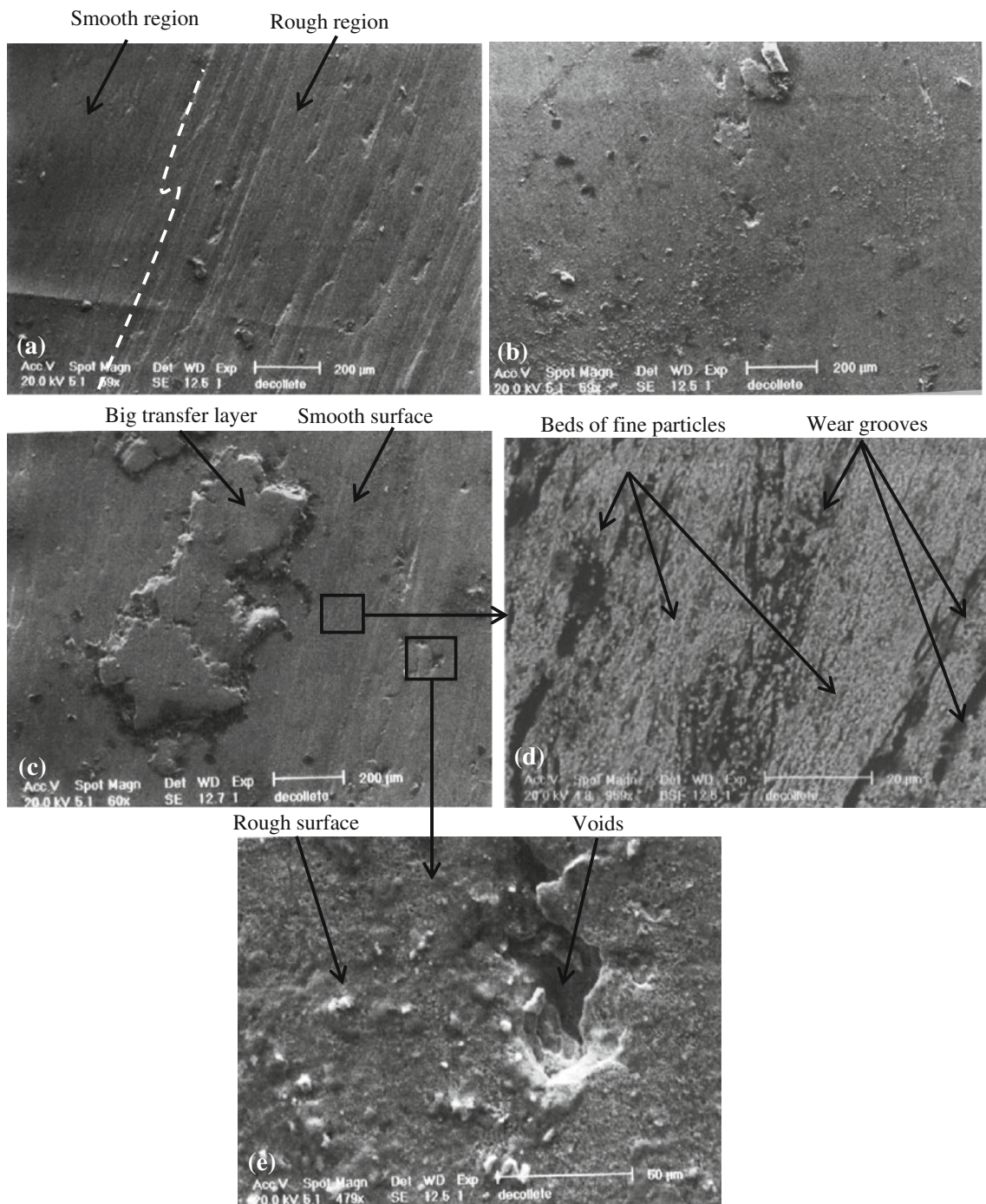


**Fig. 11** SEM observations of Md brass surface: (a) and (b) smooth and rough rubbed surface, (c) identification of a large transfer layer, (d) beds of fine particles, (e) void on a rough surface



the disk and the accumulation of brass on the surface of the pin.

On the rubbed surface of Mm brass, two distinct zones are observed: a smooth zone with some wear debris with a particle board (see Fig. 10a) and the other zone full of agglomerated particles (see Fig. 10b). The maximum size of these particles can reach 200  $\mu\text{m}$ . The details of this zone show a scratched surface (see Fig. 10c). Figure 11 shows SEM observations of some regions of the rubbed surface of Md brass. This surface is relatively particulate than the other brass in the fashion and wear mechanisms. Indeed, beds of very fine particles fill the grooves, forming a smooth region which covers most of the surface. A large transfer layer is also detected in the center of the friction trace. The size of this layer exceeds 600  $\mu\text{m}$  in length, spread in the direction of slip.

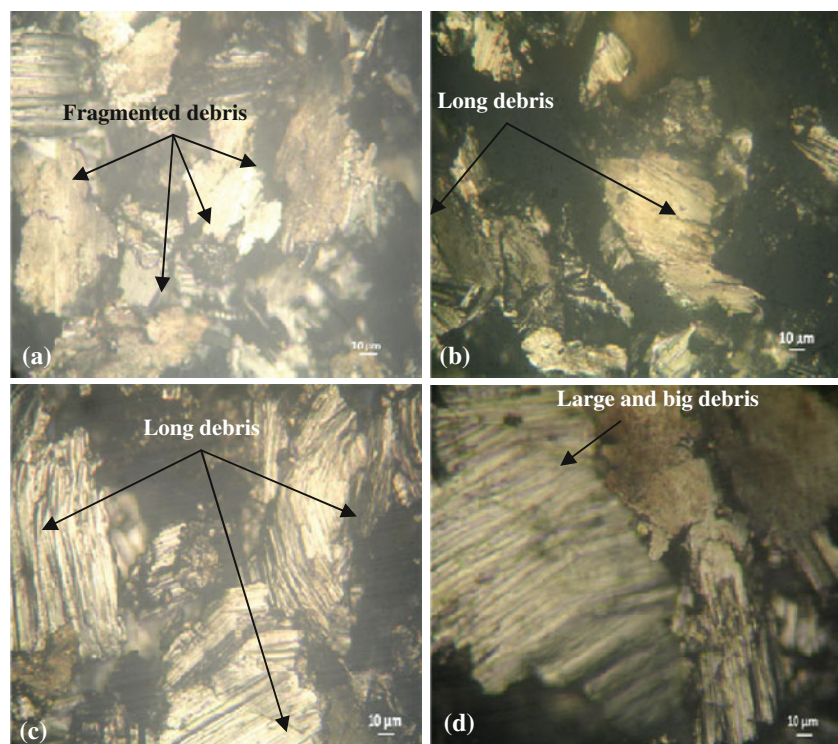
For all brass alloys, the debris is made up of intimate mixture of small particles essentially from brass materials. Loose debris has been reported to have the same structure and composition as that of the transfer layer and is expected to be formed by delamination of the transfer layer (see Fig. 12). For the Mc alloy, the debris is generally small and spherical with a mean size of 50  $\mu\text{m}$  (see Fig. 12a). They are found to be metallic with the presence of oxide particles. The existence of crack marks on the surface may be due to a fragmentation mechanism of debris, which could be generated by hard particles like

oxide and oxidized third bodies. For the Mm alloy, the debris has a length up to 100  $\mu\text{m}$  (see Fig. 12b). For the Mi alloy, a large amount of flake-type debris is detected. Their length is about 120–150  $\mu\text{m}$  with a width of 50–60  $\mu\text{m}$ . This aspect suggests that delamination is the predominating mechanism for this material (see Fig. 12c). For the Md alloy, wear debris particles are longer than the others (see Fig. 12d).

As it is known, the typical characteristics of the “third bodies” are as follows: they flow; they transmit load; they separate or screen the “first bodies”; they accommodate velocity gradients; they can be created, destroyed, and regenerated during sliding; they can be hard or soft and can range from localized particles to a continuous layer; and their behavior depends on the dimensions, composition, and properties which may be close to the materials’ limit [12]. Different shapes and forms for “third bodies” are found. This confirms that the forming process influences their appearance in different material systems: For the Mc alloy, it is a “transfer layer,” for the Mm and Mi alloys it is a “third layer,” and for the Md alloy it is a “mechanically mixed layer.”

A cross-sectional examination of the worn surface revealed the presence of different layers in the subsurface for the Mm, Mi, and Md alloys (see Fig. 13). The optical observation revealed the formation of a heavily deformed layer, about 50  $\mu\text{m}$  thick for Mm and 200  $\mu\text{m}$  for Mi alloys (see Figs. 13a and 12b, respectively), beneath the surface

**Fig. 12** Observations of debris; (a) Mc, (b) Mm, (c) Mi, (d) Md



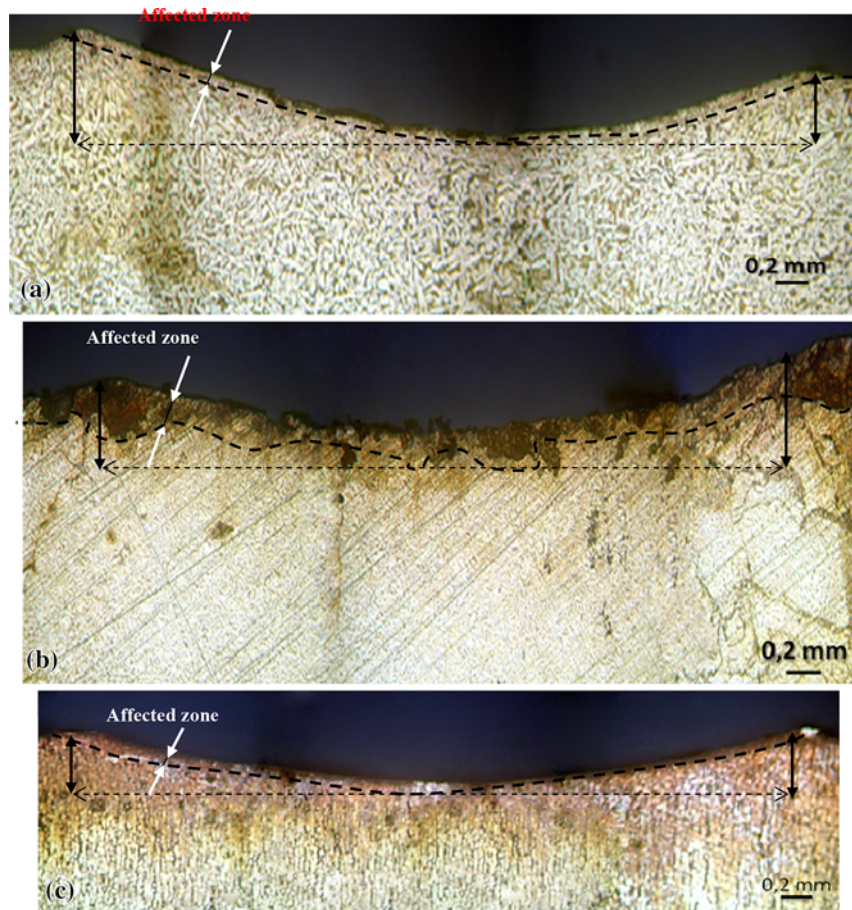


**Fig. 13** Cross-sectional observations of disk and wear crater measurement: (a) Mm, (b) Mi, (c) Md

and identified by numerous slip traces on an etched surface. Figure 13c shows an irregular deformed layer for the Mi alloy and numerous voids are found on this layer. It is interesting to notice that voids are often aligned parallel to the sliding surface with no crack in their proximity. By comparing the depth of the sliding mark of the pin, it was noted that they vary from one brass alloy to another; it is about 4, 3.5, and 3 mm for Mc, Mi, and Md alloys, respectively. This observation is coherent with the result of the weight loss. Therefore, one can suggest that ductility and voids play a great role on the wear mechanisms of brass alloys.

With an optical microscope, it is observed that the transfer of brass on steel is composed of very fine brass particles for all the samples. During sliding, it is remarked that after only few revolutions of the disk, it deposits an amount of brass on the pin. Owing to the ductility of brass, the valleys of grooves are filled with an important quantity of brass that is transferred to the pin surface. The observations with the optical microscope showed that this film is generally thin and uniform over almost the entire surface

for all the specimens. Wear particles transferred with an average radius of 400  $\mu\text{m}$ . For the Mc alloy, particles are oxidized. The process of the transfer particles can be explained as following: Before the wear, the particles are produced from the rubbing surface; they grow as transfer particles. The brass material is thus transferred to the other asperity and becomes a transfer particle. At the next contact of the same transfer particle with another asperity of brass surface, the asperity will be sheared and will adhere on the initial transfer particle. This adherence increases the thickness of the transfer particles. With the increase of contact temperature, the debris is oxidized and becomes harder to act strongly on the disk surface. An abrasive wear mechanism takes place. The development of transfer particles follows this process during the sliding motion. After each new contact, transfer particle/brass asperity, the contact shears the new asperity to give a new transfer particle or eject the asperity on wear debris. A mechanism of growth and fragmentation of debris eats the contact with third bodies. This scenario can justify the elevation of wear of the Mc alloys.

## Conclusions

From the results and discussion, the following conclusions can be drawn:

1. The coefficient of friction versus time curves showed similar characteristics for all the brass alloys: a transient period followed by a single steady-state regime. Moreover, the mean value of the coefficient of friction is 0.3 for all brass alloys. Only the Md sample showed a stabilized friction coefficient, especially at the end of the test.
2. The analysis of the surface morphology by optical micrographs suggests abrasive wear mechanisms, especially for the Mc brass alloy. Debris particles also appear to stick to the surface.
3. Two types of debris particles were observed in the present study, fine equiaxed particles with size ranges from a few  $\mu\text{m}$  to less than 1  $\mu\text{m}$  and large flakes with length = 400  $\mu\text{m}$ , suggesting a bimodal distribution of the debris particles. The oxidation of debris faded the sliding contacts with hard particles for the Mc alloy and accelerated the abrasive wear.

**Acknowledgments** The authors duly acknowledge the support and contribution of the SOPAL Society employees and thank them for their cooperation and assistance in the preparation of samples for laboratory analysis.

## References

1. H. Mindivan, H. Çimenoğlu, E.S. Kayali, Microstructures and wear properties of brass synchroniser rings. *Wear* **254**, 532–537 (2003)
2. E. Feyzullahoğlu, A. Zeren, M. Zeren, Tribological behaviour of tin-based materials and brass in oil lubricated conditions. *Mater. Des.* **29**(3), 714–720 (2008)
3. C.N. Panagopoulos, E.P. Georgiou, K. Simeonidis, Lubricated wear behavior of leaded  $\alpha + \beta$  brass. *Tribol. Int.* **50**, 1–5 (2012)
4. J.P. Davim, An experimental study of tribological behaviour of brass/steel pair. *J. Mater. Process. Technol.* **100**, 273–277 (2000)
5. M. Amira, H. Zaidia, A. Djamaia, D. Neciba, D. Eyidib, Influence of the gas environment on the transferred film of the brass (Cu64Zn36)/steel AISI 1045 couple. *Wear* **267**, 433–440 (2009)
6. M.F. Buchely, J.C. Gutierrez, L.M. Leon, A. Toro, The effect of microstructure on abrasive wear of hardfacing alloys. *Wear* **259**, 52–61 (2005)
7. K. Elleuch, R. Elleuch, R. Mnif, V. Fridrici, P. Kapsa, Sliding wear transition for the CW614 brass alloy. *Tribol. Int.* **39**, 290–296 (2006)
8. Mnif, R., Elleuch, K., Elleuch, R., Fridrici, V., Kapsa, P.: Thermal effect on wear behaviour of copper alloys. In: Second International Conference ICAMEM, Hammamet (2004)
9. T.A. Stolarski, *Tribology in Machine Design* (Butterworth/Heinemann, Oxford, 2000)
10. A.B. Aghdam, M.M. Khonsari, On the correlation between wear and entropy in dry sliding contact. *Wear* **270**(11–12), 781–790 (2011)
11. W.X. Qi, J.P. Tu, F. Liu, Y.Z. Yang, N.Y. Wang, H.M. Lu, X.B. Zhang, S.Y. Guo, M. Liu, Microstructure and tribological behaviour of a peak aged Cu–Cr–Zr alloy. *Mater. Sci. Eng.* **A343**, 89–96 (2003)
12. A. Williams John, Wear and wear particles—some fundamentals. *Tribol. Int.* **38**, 863–870 (2005)
13. S. Kalpakjian, S.R. Schmid, *Manufacturing Processes for Engineering Materials*, 4th edn. (Prentice Hall, Upper Saddle River, 2003), p. 197
14. F.A. Sadykov, N.P. Barykin, I.R. Aslanyan, Wear of copper and its alloys with submicrocrystalline structure. *Wear* **225–229**, 649–655 (1999)
15. J.P. Tu, L. Meng, M.S. Liu, Friction and wear behavior of CuFe3Al powder metallurgical composites in dry sliding. *Wear* **220**, 72–79 (1998)